Supporting Information

Enhancing H_2O_2 and Glucose Double Detection by Surface Microstructure Regulation of Brussels Sprouts-Like Ni-$Co(OH)_2$/rGO/Carbon Cloth Composite

Xinmeng Zhang,[*a] Zixuan Mao,[a] Wanyin Ge,[a] Jiajing Zhu,[a] Yuanxiao Zhao[b]

[a]School of Materials Science and Engineering, Shaanxi Key Laboratory of Green Preparation and Functionalization for Inorganic Materials, Shaanxi University of Science & Technology, Xi'an, 710021, China

[b]State Key Laboratory of Solidification Processing, Carbon/Carbon Composites Research Center, Northwestern Polytechnical University, Xi'an, 710072, China

Author Information

***Corresponding Author**: Xinmeng Zhang,

E-mail Address: zhangxinmeng12@126.com

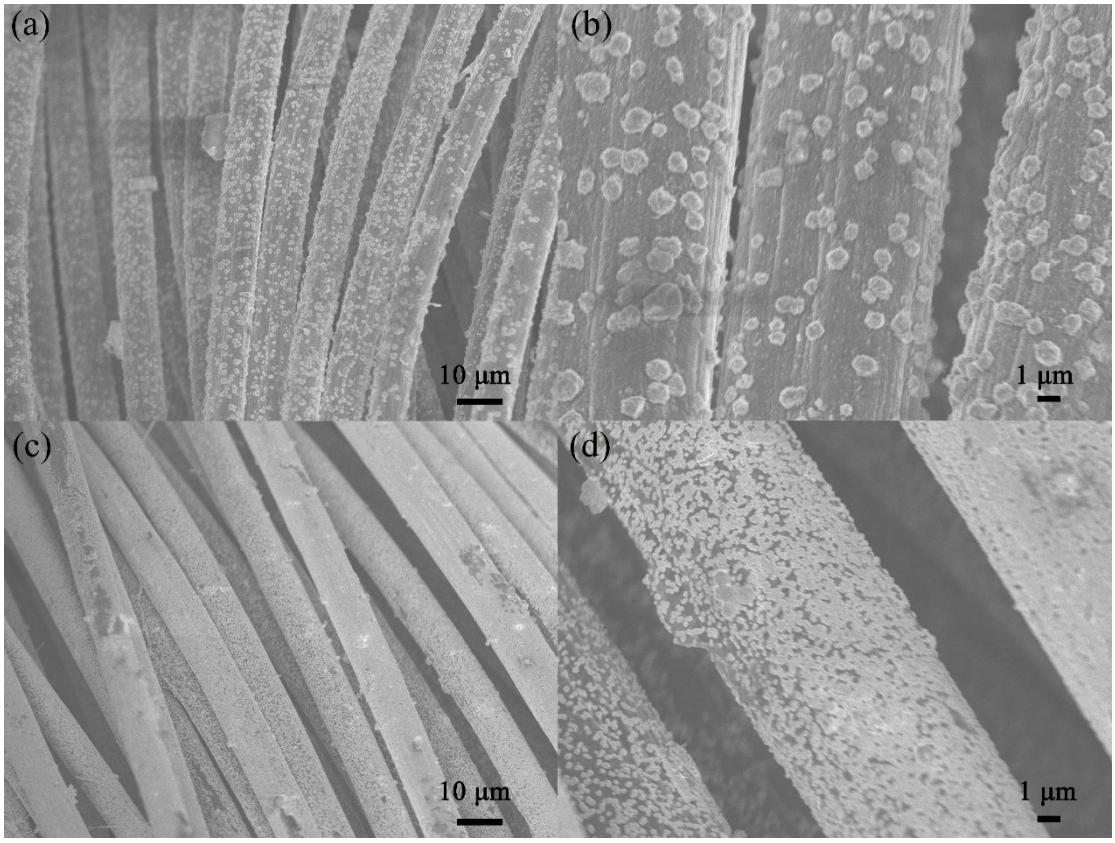

Fig. S1 (a, b) SEM images of the $Co(OH)_2$/CC and (c, d) Ni/CC composites.

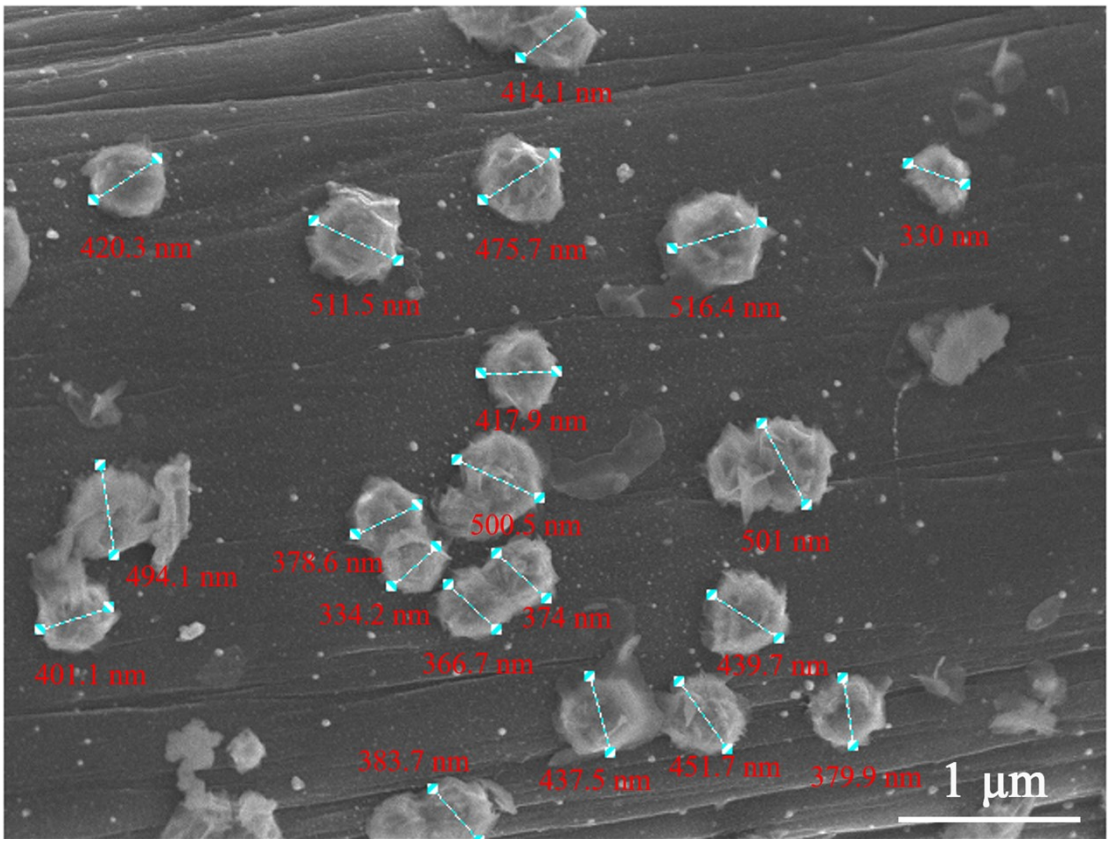

Fig. S2 SEM image of the Ni-Co(OH)$_2$/rGO/CC composite and the measurement results of diameters of Ni-Co(OH)$_2$ microparticles.

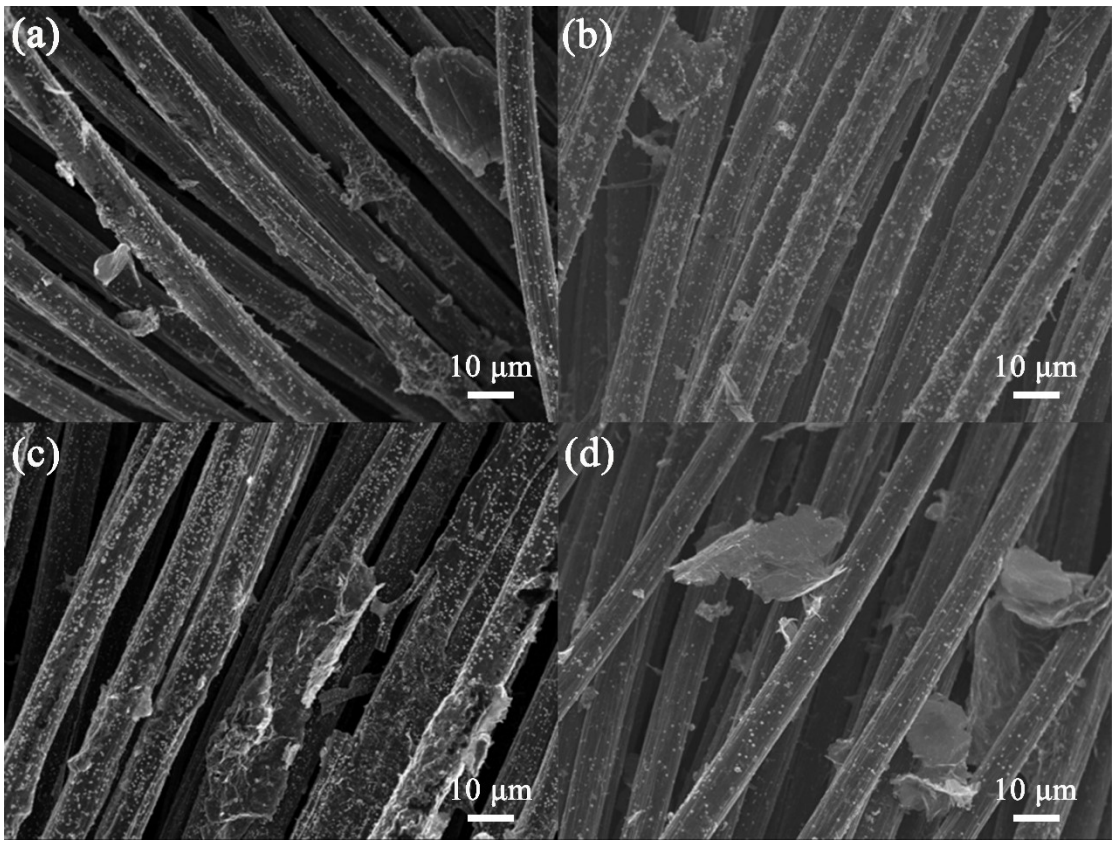

Fig. S3 SEM images of (a) Ni-$Co(OH)_2$/rGO1/CC, (b) Ni-$Co(OH)_2$/rGO2/CC, (c) Ni-$Co(OH)_2$/rGO3/CC, and (d) Ni-$Co(OH)_2$/rGO4/CC composites.

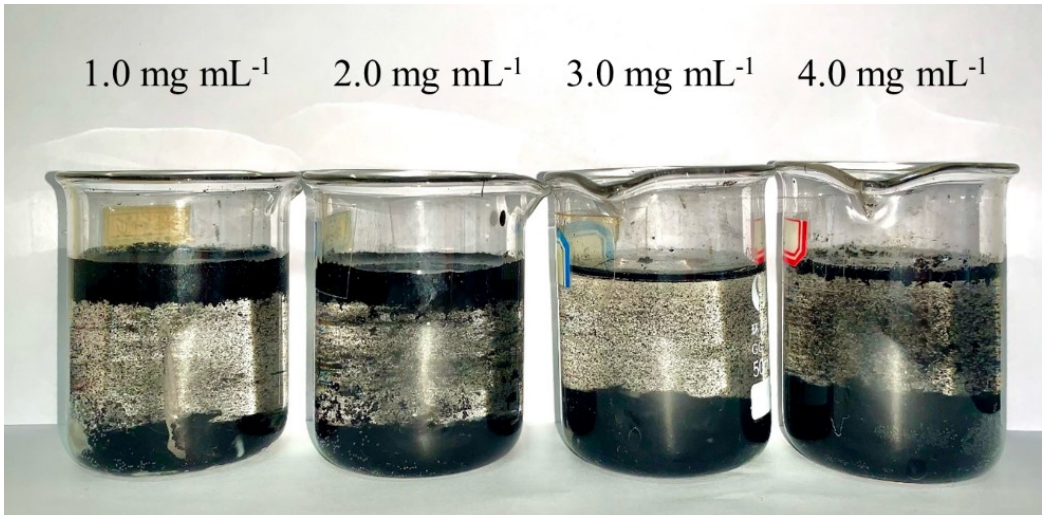

Fig. S4 Digital photograph of Ni-$Co(OH)_2$/rGO/CC composites in aqueous solution with different content of rGO after the hydrothermal reaction.

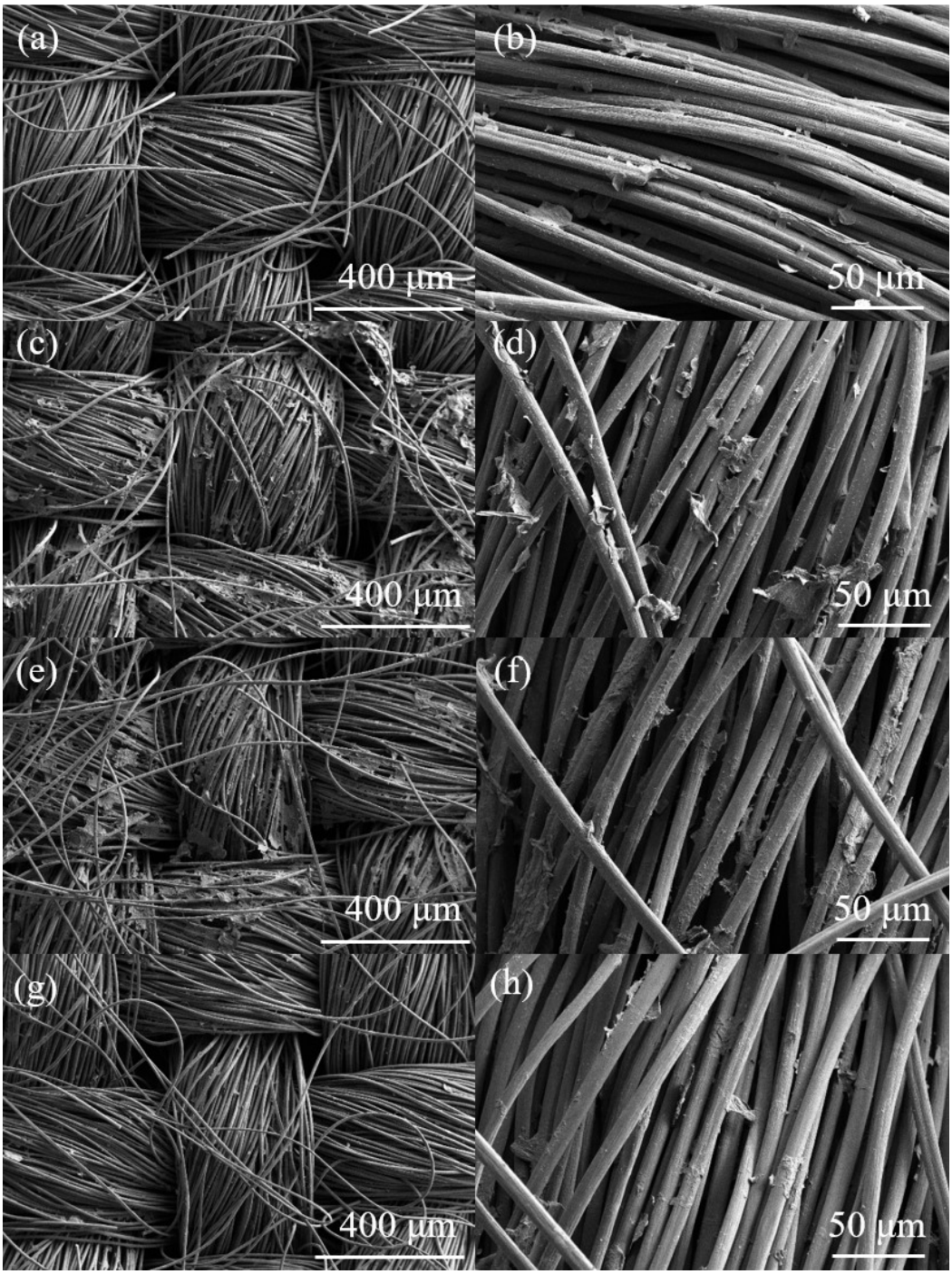

Fig. S5 The FE-SEM images of rGO/CC composites with (a, b) 1.0, (c, d) 2.0, (e, f) 3.0, and (g, h) 4.0 mg mL^{-1} content of rGO with different magnification.

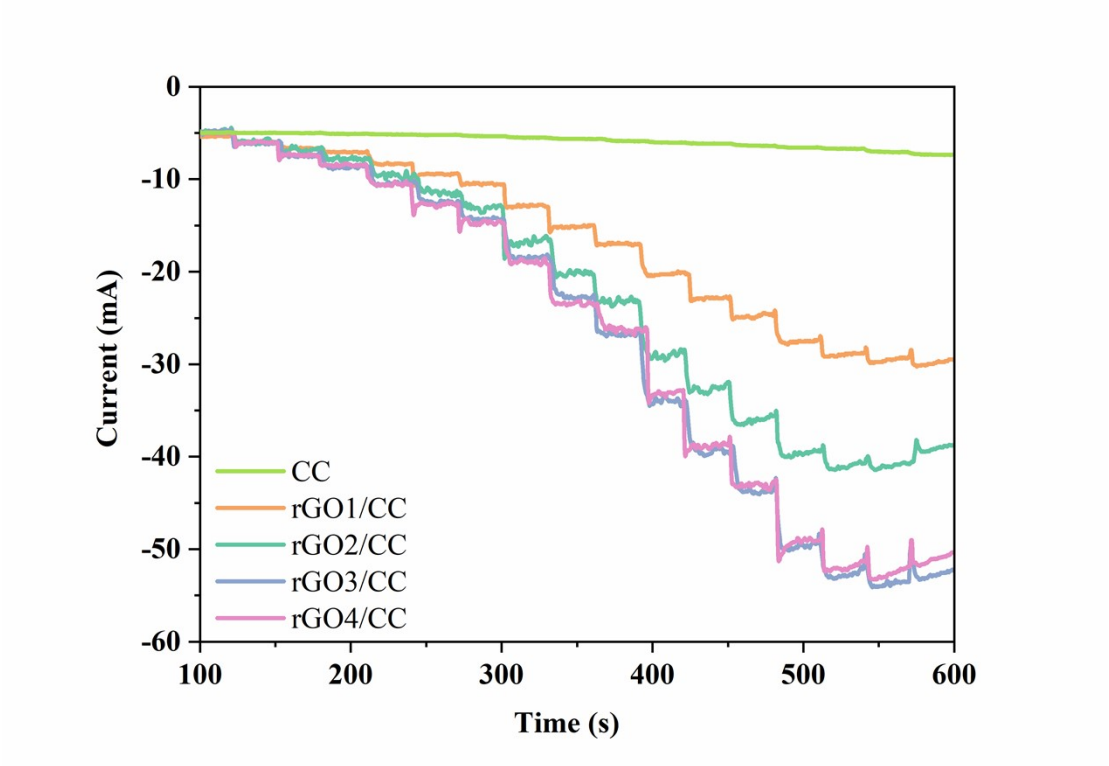

Fig. S6 I-t curves of the rGO/CC electrodes were prepared by different content of rGO (1.0, 2.0, 3.0, and 4.0 mg mL^{-1}) with the successive addition of different concentrations of H_2O_2 at -0.57 V.

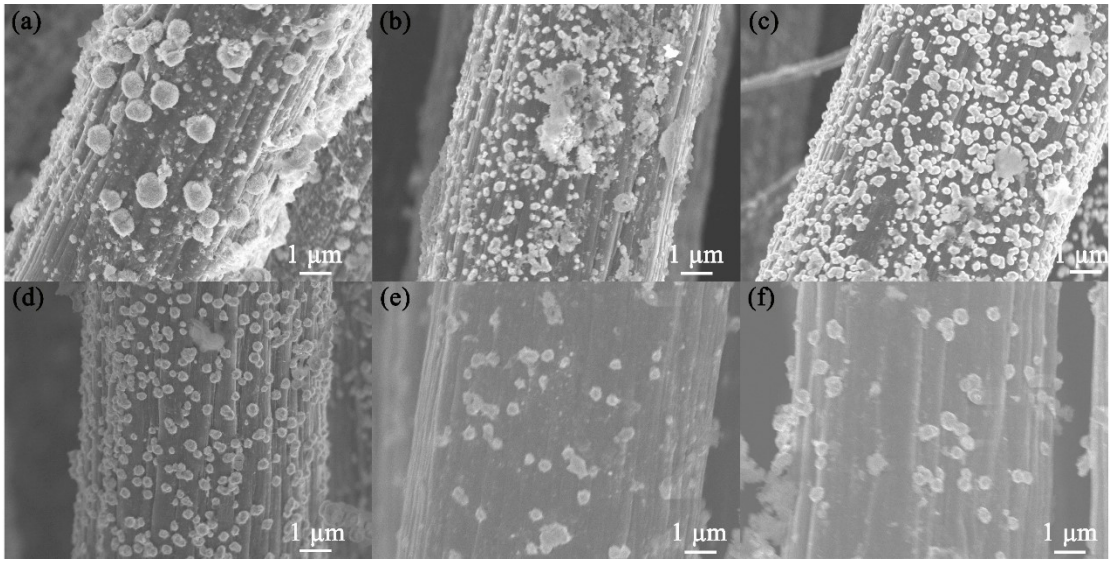

Fig. S7 The SEM images of Ni-Co$(OH)_2$/rGO3/CC composites with hydrothermal reaction time: (a) 3 h, (b) 6 h, (c) 9 h, (d) 12 h, (e) 18 h, and (f) 24 h (The other experimental conditions remain unchanged).

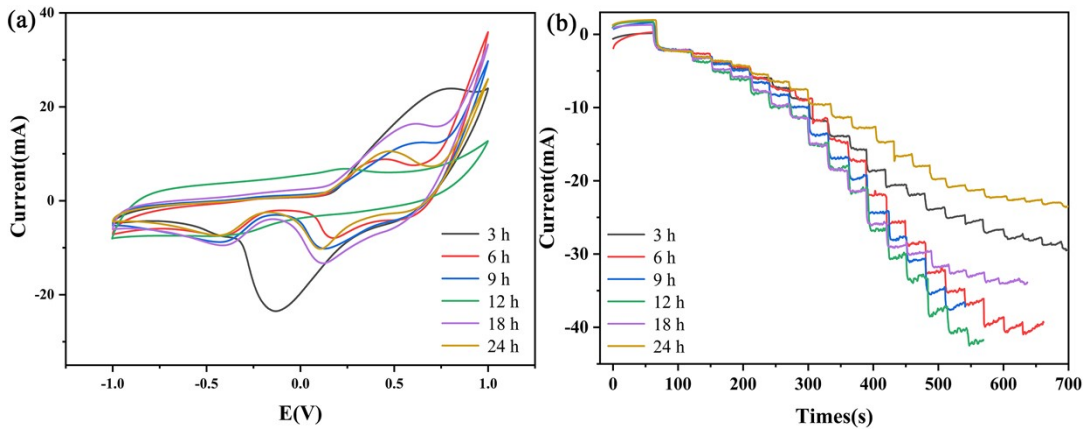

Fig. S8 (a) The CVs of Ni-Co(OH)$_2$/rGO3/CC electrodes with different hydrothermal reaction times at the scan rate of 50 mV·s^{-1}. (b) I-t curves of the Ni-Co(OH)$_2$/rGO3/CC electrodes were prepared with different hydrothermal reaction times by the successive addition of different concentrations of H_2O_2 at –0.57 V.

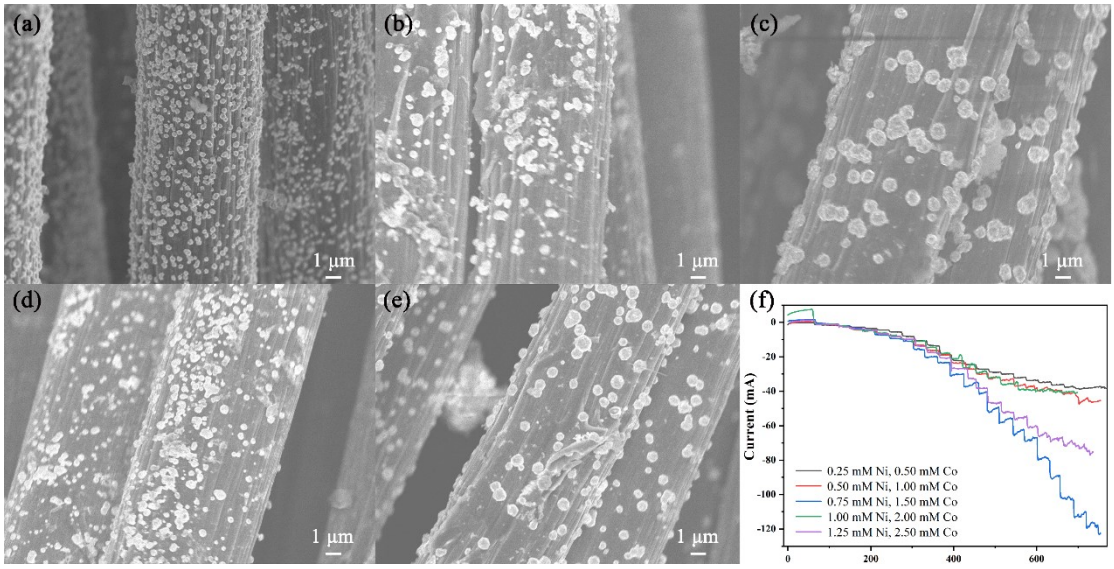

Fig. S9 The SEM images of the content with (a) Ni is 0.25 mM, and Co is 0.50 mM; (b) Ni is 0.50 mM, and Co is 1.00 mM; (c) Ni is 0.75 mM, and Co is 1.50 mM; (d) Ni is 1.00 mM, and Co is 2.00 mM; (e) Ni is 1.25 mM, and Co is 2.50 mM. (f) I-t curves of the Ni-Co$(OH)_2$/rGO3/CC electrodes with different concentrations of Ni and Co with the successive addition of different concentrations of H_2O_2 at -0.57 V (The other experimental conditions remain unchanged).

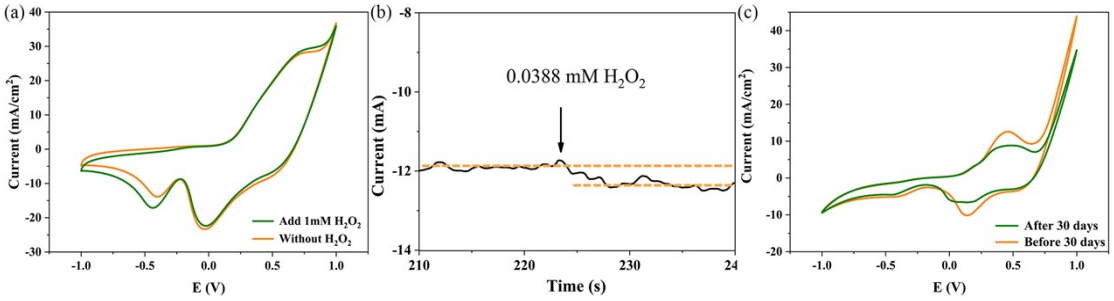

Fig. S10 (a) The CVs of Ni-Co(OH)$_2$/rGO3/CC electrodes in the presence and absence of 1 mM H_2O_2 at -0.57 V. (b) The lowest concentration can be detected of Ni-Co(OH)$_2$/rGO3/CC electrode in the experiment. (c) The CVs of Ni-Co(OH)$_2$/rGO3/CC electrode before and after 30 days of storage at room temperature.

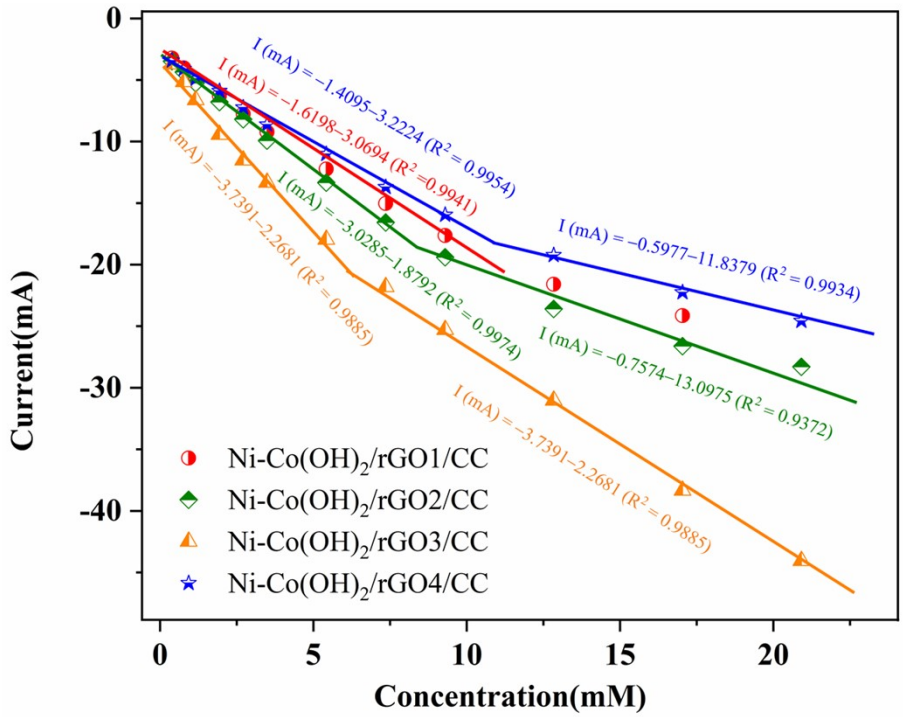

Fig. S11 The corresponding calibration curves and calibration equations of Ni-Co(OH)$_2$/rGO1/CC, Ni-Co(OH)$_2$/rGO2/CC, Ni-Co(OH)$_2$/rGO3/CC, and Ni-Co(OH)$_2$/rGO4/CC composites.

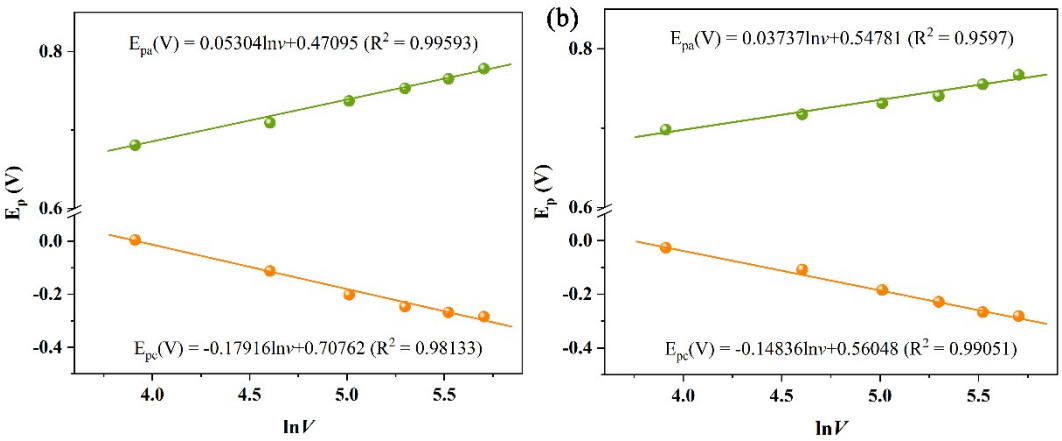

Fig. S12 The variation trends of the peak potential versus the natural logarithm of scan rate for detection (a) H_2O_2 and (b) glucose.

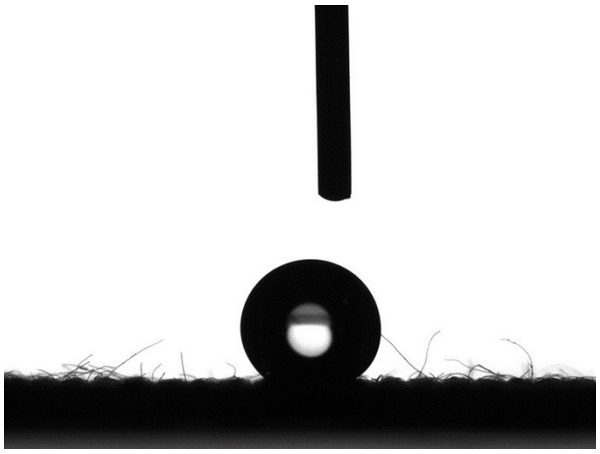

Fig. S13 The distribution of 5 μL water droplet on CC without hydrothermal reaction and the surface water contact angle is 143.0°.

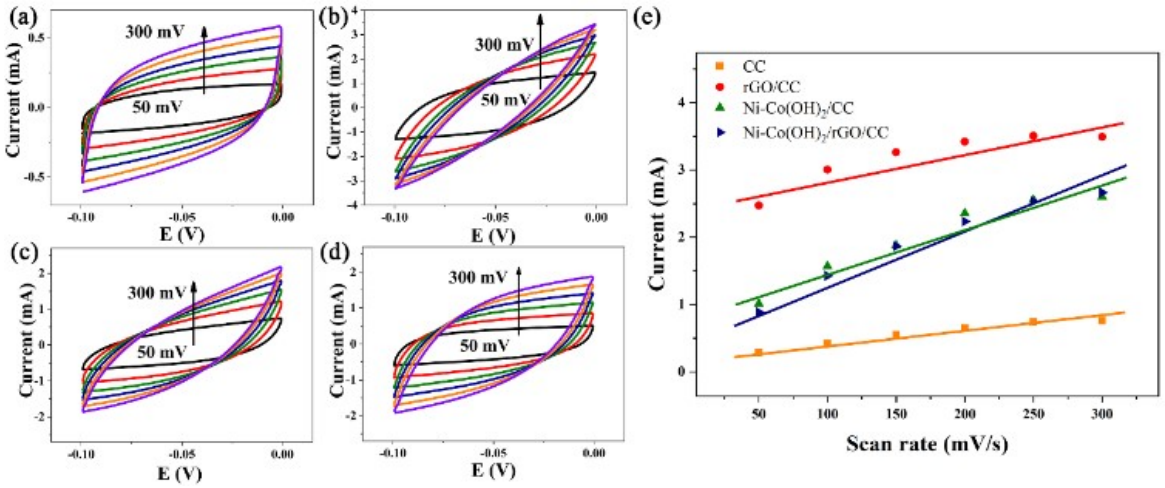

Fig. S14 The CVs of (a) CC, (b) rGO/CC, (c) Ni-Co(OH)$_2$/CC, and (d) Ni-Co(OH)$_2$/rGO/CC electrodes were performed from −0.1 to 0 V with different scan rates. (e) Current versus scan rates based on the CVs curves of (a-d) at a voltage of −0.05 V.

Table S1 EIS relevant data of Ni-$Co(OH)_2$/rGO/CC electrodes with different content of rGO.

Samples	R_s (Ω)	R_{ct} (Ω)	W_o-R (Ω)
Ni-$Co(OH)_2$/CC	32.69	34.33	31.66
Ni-$Co(OH)_2$/rGO1/CC	25.14	19.42	14.36
Ni-$Co(OH)_2$/rGO2/CC	22.25	17.23	7.00
Ni-$Co(OH)_2$/rGO3/CC	22.65	17.22	13.66
Ni-$Co(OH)_2$/rGO4/CC	24.90	20.53	13.06

Table S2 Sensing performance of H_2O_2 sensor in a recently reported.

The test materials	Detection limit (μM)	Sensitivity (mA cm^{-2} mM^{-1})	References
AuPt/MOF-Graphene	0.019	0.006	[35]
Ag/M-ZIF	1.100	0.420	[36]
Ag/Fe	0.100	1.350	[37]
$NiCo_2N$/NG	0.050	0.002	[38]
Au/MnO	0.080	0.208	[39]
$NiCo_2O_4$RMNs@PEDOT/rGO	0.031	0.679	[40]
AuNPs-N-GQDs	0.120	0.186	[41]
Ni-$Co(OH)_2$/rGO3/CC	0.002	3.739	This work

Table S3 Sensing performance of glucose sensor in a recently reported.

The test materials	Detection limit (μM)	Sensitivity (mA cm^{-2} mM^{-1})	References
graphene@ZIF	0.360	1.521	[43]
NiO nanostructures	0.500	0.004	[44]
NCAG/Fe	0.530	2.455	[45]
NBC/GCE	0.041	0.416	[46]
NiS	0.052	0.006	[47]
NiCo LDH/GCE	0.011	0.166	[12]
3D graphene/Co_3O_4	0.025	3.390	[48]
Ni-$Co(OH)_2$/rGO3/CC	0.115	1.846	This work

Table S4 C_{dl} and ECSA values of different electrodes in 0.1 M KOH.

Electrodes	C_{dl} (mF)	ECSA (cm^2)
CC	1.960	110.274
rGO/CC	4.378	246.249
Ni-$Co(OH)_2$/CC	6.508	366.068
Ni-$Co(OH)_2$/rGO/CC	7.189	404.372